Sample-specific conductance fluctuations modulated by the superconducting phase

Hartog , den, Sander; Kapteyn, C.M.A.; Wees, B.J. van; Klapwijk, T.M.; Borghs, G.

Published in:
Physica B: Condensed Matter

DOI:
10.1016/S0921-4526(98)00170-7

ELSEVIER

Physica B 249–251 (1998) 485–489

PHYSICA B

Sample-specific conductance fluctuations modulated by the superconducting phase

S.G. den Hartog[a], C.M.A. Kapteyn[a], B.J. van Wees[a], T.M. Klapwijk[a,*], G. Borghs[b]

[a] *Department of Applied Physics and Material Science Centre, University of Groningen, Nijenborgh 4, 9747 AG Groningen, The Netherlands*
[b] *Interuniversity Micro Electronics Centre, Kapeldreef 75, B-3030 Leuven, Belgium*

Abstract

We present an overview of sample-specific transport properties tuned by the superconducting phase difference between two superconductors connected to a disordered 2-dimensional electron gas (2DEG). We demonstrate a crossover from ensemble-averaged to sample-specific resistance oscillations of a T-shaped 2DEG interferometer by increasing the magnetic field. Multi-terminal resistances of a cross-shaped 2DEG interferometer are analyzed in terms of an extended Landauer–Büttiker transport formalism. We show that the extended reciprocity relations hold and that three-terminal resistances become negative.

Keywords: Superconducting proximity effect; Universal conductance fluctuations

In a disordered phase-coherent normal conductor, small compared to the phase-breaking length l_φ but larger than the elastic scattering length l_e, electron waves are scattered and can interfere [1]. This interference pattern and hence the conductance is sensitive to a change in Fermi-energy, position of the scatterers or magnetic flux. For a specific conductor, the fluctuations in the conductance (UCF) are reproducible and have an universal rms magnitude $\delta G \simeq e^2/h$.

An interesting question is the possible influence of the macroscopic phase of the superconductor on the conductance fluctuations of a disordered normal conductor [2,3]. During the process of Andreev reflection an incoming electron wave is converted into an Andreev reflected hole wave at the NS-interface, which is accompanied by a shift in its phase equal to the superconducting phase. In this paper, we will highlight several sample-specific transport properties observed in disordered 2-dimensional electron gas (2DEG) Andreev interferometers.

We have designed two types of interferometers by coupling an interrupted superconducting loop to either a T-shaped or cross-shaped disordered 2DEG (see Figs. 1 and 4, respectively). The fabrication processes are described in Refs. [4,5], respectively. The transport properties of the 2DEG are

* Corresponding author. Tel.: + 31 50 3634930; fax: + 31 50 3633900; e-mail: klapwijk@phys.rug.nl.

0921-4526/98/$19.00
PII: S0921-4526(98)00170-7

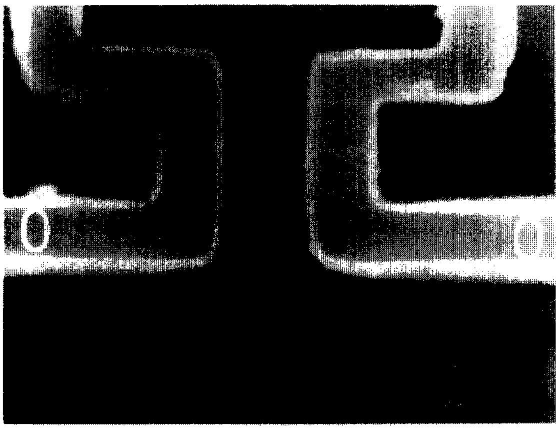

Fig. 1. Scanning electron micrograph of a T-shaped interferometer. The contacts (0) are connected to the niobium loop and (1) and (2) are connected to the T-shaped 2DEG.

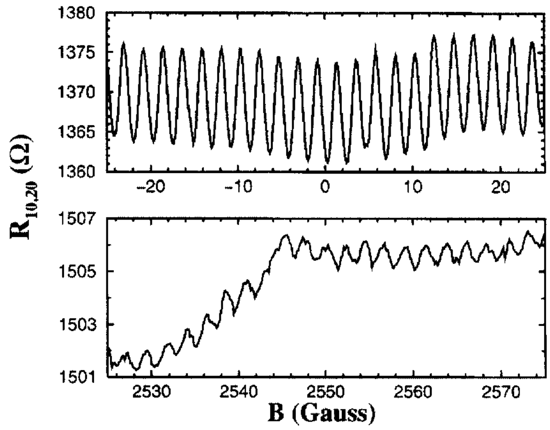

Fig. 2. The magnetoresistance $R_{10,20}$ at 50 mK of the T-shaped interferometer around zero magnetic field (top panel) and in the presence of about 50 flux quanta h/e through the total T-shaped 2DEG (bottom panel).

$n_s \simeq 1.3 \times 10^{16}\ \mathrm{m}^{-2}$ and an electron mean free path $l_e \simeq 0.2\ \mu\mathrm{m}$. For the cross-shaped interferometer the presence of an insulating Si layer between the contacts to this cross-shaped 2DEG and the Nb superconducting loop is essential to prevent a short-circuit. Note that the 2DEG-superconductor interface is highly transparent due to Ar cleaning of the exposed 2DEG regions before Nb deposition.

We have studied three T-shaped interferometers at a temperature of 50 mK with a standard 4-probe AC lock-in technique and filtered leads. Fig. 2 displays the observed magnetoresistance $R_{10,20}$. Here, the current is injected by one of the contacts (1,2) and extracted by one of the superconducting contacts (0). The voltage difference is measured between the two remaining contacts. The effect of the applied magnetic field is twofold. First, the phase difference $\Delta\phi$ between the two superconducting electrodes is changed according to: $\Delta\phi = 2\pi\Phi/\Phi_0$, where Φ is the applied flux through area A ($\approx 10.3\ \mu\mathrm{m}^2$) confined by the Nb loop and the T-shaped 2DEG and $\Phi_0 \equiv h/2e$. Second, the magnetic field penetrates the T-shaped 2DEG. In the upper panel of Fig. 2 the magnetoresistance $R_{01,02}$ around zero Gauss is shown. These low-field oscillations have a magnitude $\delta G_{qp} \simeq 0.20e^2/h$ and a period $h/2e$, which corresponds is an increase of $\Delta\phi$ by 2π. For these oscillations coherence between electrons and Andreev reflected holes is essential [6]. They are independent of the specific impurity configuration and therefore survive ensemble-averaging. These quasiparticle interference oscillations disappear when about one flux quantum h/e penetrate the T-shaped 2DEG, which occurs at about 120 Gauss.

Remarkably, the oscillations do not completely disappear for magnetic fields corresponding with several flux quanta through the total T-shaped 2DEG (Fig. 2 panel b). The rms magnitude of these high-field oscillations is $\delta G_{\Delta\phi} \simeq 0.01e^2/h$ and the period is $h/2e$. By averaging over one period a fluctuating background resistance is obtained. In Fig. 3, the data are shown after subtracting the fluctuating background resistance, leaving the $h/2e$ oscillations. The crossover from low-field quasiparticle oscillations to high-field oscillations around 120 G is evident. The other two nominally identical devices showed a similar behavior at low magnetic fields. However, the amplitude and phase of both the high-field superconductor-modulated conductance oscillations and the fluctuations in the background resistance were uncorrelated. Therefore, we attribute these high-field oscillations to be sample-specific conductance fluctuations tuned by the phase difference across the two superconducting boundaries.

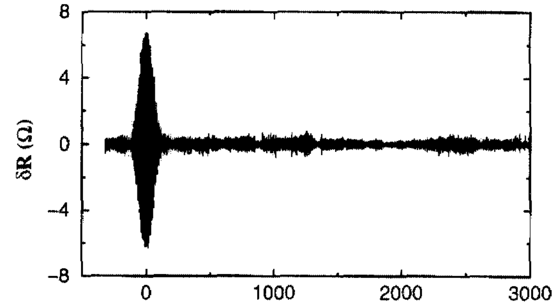

Fig. 3. Oscillations in the magnetoresistance $R_{10,20}$ at 50 mK.

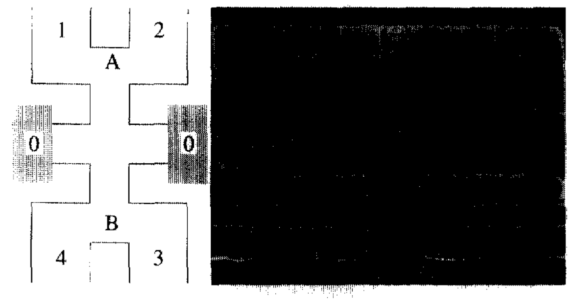

Fig. 4. Sample layout. The left-hand panel shows a schematic picture of the cross-shaped 2DEG (contacts 1,2,3, and 4) with the superconducting terminals (0). The right-hand panel shows a scanning electron micrograph.

We proceed with investigating multi-terminal transport in the cross-shaped interferometer (Fig. 4). A multi-terminal scattering approach has been proposed for transport in NS-devices [7] based on an extension of the Landauer–Büttiker transport formalism, including Andreev transmission and reflection coefficients (T_{ij}^{he}, R_{ii}^{he}). The current flowing in lead i is expressed as: $I_i = 2e/h((N_i - R_{ii}^{ee} + R_{ii}^{he})\mu_i - \sum_{j\neq i}(T_{ij}^{ee} - T_{ij}^{he})\mu_j)$. Particle conservation implies: $N_i = R_{ii}^{ee} + R_{ii}^{he} + \sum_{j\neq i}(T_{ij}^{ee} + T_{ij}^{he})$, where N_i denotes the number of quantum channels. We will describe regions A and B as reservoirs, assuming uniform electrochemical potentials $\mu_A = \mu_1 = \mu_2$ and $\mu_B = \mu_3 = \mu_4$ where $\mu_0 = 0$.

We first derive an expression for the multi-terminal resistances for the geometry shown in Fig. 4. We define the transport coefficients as the difference between the normal and Andreev transmission/reflection coefficients: $T_{ij} = T_{ij}^{ee} - T_{ij}^{he}$ and $R_{ii} = R_{ii}^{ee} - R_{ii}^{he}$. We then obtain:

$$\mathscr{R}_{10,20} = \frac{h}{2e^2}\frac{N - R_{BB}}{(N - R_{AA})(N - R_{BB}) - T_{AB}T_{BA}},$$

$$\mathscr{R}_{30,40} = \frac{h}{2e^2}\frac{N - R_{AA}}{(N - R_{AA})(N - R_{BB}) - T_{AB}T_{BA}},$$

$$\mathscr{R}_{10,30} = \frac{h}{2e^2}\frac{T_{BA}}{(N - R_{AA})(N - R_{BB}) - T_{AB}T_{BA}},$$

$$\mathscr{R}_{30,10} = \frac{h}{2e^2}\frac{T_{AB}}{(N - R_{AA})(N - R_{BB}) - T_{AB}T_{BA}}.$$

The number of quantum channels is given by $N = k_F W/\pi$, where W is the width of the arms of the cross. The first two resistances are referred to as being "two-terminal", since they effectively measure the resistance between region A (or B) and the Nb electrodes. The last two resistances are "three-terminal" resistances, since they involve both regions A and B and the Nb electrodes.

Time-reversal symmetry implies for the transport coefficients that: $T_{ij}(\Phi, \Delta\varphi) = T_{ji}(-\Phi, -\Delta\varphi)$ and $R_{ii}(\Phi, \Delta\varphi) = R_{ii}(-\Phi, -\Delta\varphi)$ [7], where Φ is the magnetic flux through the conductor and $\Delta\varphi$ is the superconducting phase difference across the two Nb terminals. The reciprocity relations can be derived from the extended Landauer–Büttiker formalism: $\mathscr{R}_{ij,kl}\ (\Phi, \Delta\varphi) = \mathscr{R}_{kl,ij}\ (-\Phi, -\Delta\varphi)$. Interchanging current and voltage leads accompanied by a sign reversal in *both* Φ *and* $\Delta\varphi$ is predicted to yield the same resistance.

The magnetoresistances for the two and three-terminal configurations are shown in Fig. 5. The magnetoresistance shows superconducting phase modulated conductance fluctuations [2,4,5], superimposed on a fluctuating background resistance. At low magnetic fields (< 100 G) a non sample-specific (ensemble-averaged) contribution to the resistance oscillations is present. Evidently, the two-terminal resistances $\mathscr{R}_{10,20}$ and $\mathscr{R}_{30,40}$, as shown in Fig. 5a and b, are symmetric in Φ and $\Delta\varphi$. The three-terminal magnetoresistance $\mathscr{R}_{10,30}$ (panel (c)) is asymmetric. This asymmetry is indeed reversed when the current and voltage probes are interchanged ($\mathscr{R}_{30,10}$ in panel (d)).

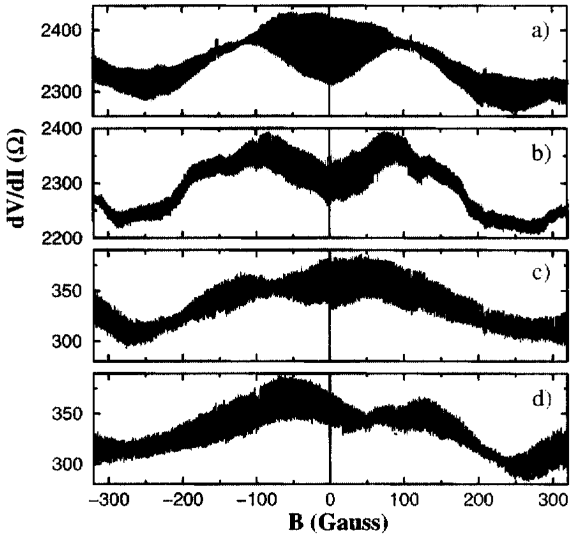

Fig. 5. The two-terminal magnetoresistances (a) $\mathscr{R}_{10,20}$ and (b) $\mathscr{R}_{30,40}$ of the cross-shaped interferometer at 100 mK are symmetric in magnetic field. The three-terminal magnetoresistance $\mathscr{R}_{10,30}$ (c) is identical to the magnetoresistance $\mathscr{R}_{30,10}$ (d) at reversed magnetic fields.

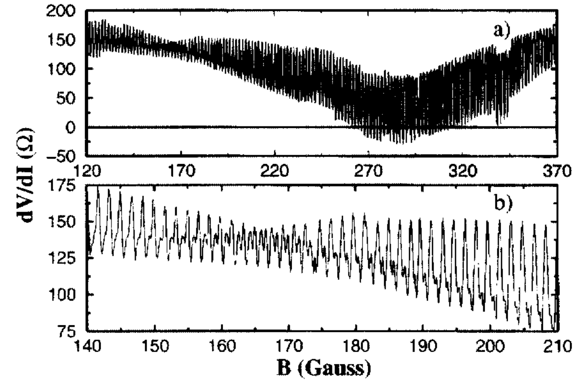

Fig. 6. (a) The three-terminal magnetoresistance $\mathscr{R}_{10,30}$ at $T \simeq 100$ mK of a cross-shaped interferometer with an increased overall resistance ($\mathscr{R}_{10,20} \simeq 10$ kΩ) becomes around 290 Gauss. In panel (b) a typical cross-over between two different Andreev-mediated sample-specific oscillation patterns is visible.

A striking manifestation of the coexistence of Andreev and normal transmission is displayed in Fig. 6a. The three-terminal resistance $\mathscr{R}_{10,30}$ is proportional to $T_{\mathrm{BA}} = T^{\mathrm{ee}}_{\mathrm{BA}} - T^{\mathrm{he}}_{\mathrm{BA}}$. This implies that when an incoming electron has an higher probability to be transmitted as an hole than as an electron ($T^{\mathrm{he}}_{\mathrm{BA}} > T^{\mathrm{ee}}_{\mathrm{BA}}$), $\mathscr{R}_{10,30}$ can become *negative* [8]. Note that negative three-terminal resistances are impossible in normal transport, since in that case a voltage probe always measures a voltage in between that of the current source and drain contacts. The three-terminal magnetoresistance becomes negative around 290 G, indicating that Andreev transmission dominates over normal transmission.

Around 170 G a crossover takes place between two different oscillation patterns (Fig. 6b). Several of these crossovers, which are sample-specific, are observed with a typical separation of ~ 160 G. This crossover cannot be described by a superposition of independent sinusoidal oscillation patterns in $T^{\mathrm{ee}}_{\mathrm{BA}}$ and $T^{\mathrm{he}}_{\mathrm{BA}}$. An estimation of their average magnitude ($\langle T^{\mathrm{ee}}_{\mathrm{BA}} \rangle \simeq 0.32$ and $\langle T^{\mathrm{he}}_{\mathrm{BA}} \rangle \simeq 0.29$ [9]) for this device shows that they are equally important. In principle, either $T^{\mathrm{ee}}_{\mathrm{BA}}$ or $T^{\mathrm{he}}_{\mathrm{BA}}$ could still dominate the amplitude of the oscillations. More likely, their amplitudes have the same order of magnitude, which implies that the crossovers should be present in both $T^{\mathrm{ee}}_{\mathrm{BA}}$ and $T^{\mathrm{he}}_{\mathrm{BA}}$. Moreover, numerical calculations [3] showed that the oscillation pattern of a chaotic Josephson junction contains a non-sinusoidal contribution when multiple Andreev scattering processes become important. These higher harmonics are responsible for the observed crossovers, which indeed occur in all individual transport coefficient (both $T^{\mathrm{ee}}_{\mathrm{BA}}$ and $T^{\mathrm{he}}_{\mathrm{BA}}$).

This work is financially supported by the stichting voor Fundamenteel Onderzoek der Materie (FOM), the Nederlandse organisatie voor Wetenschappelijk Onderzoek (NWO), and the Royal Dutch Academy of Sciences (KNAW) (B.J.v.W.).

References

[1] For a review see e.g. A.D. Stone, in: H. Heinrich, G. Bauer, F. Kuchar (Eds.), Physics and Technology of Submicron Structures, Springer, Berlin, 1988.

[2] B.L. Al'tshuler, B.Z. Spivak, Sov. Phys. JETP 65 (1987) 343; Y. Takane, H. Ebisawa, J. Phys. Soc. Jpn. 60 (1991) 3130; J. Phys. Soc. Jpn. 61 (1992) 2858; C.W.J. Beenakker, Phys. Rev. B 47 (1993) 15763; P.W. Brouwer, C.W.J. Beenakker, Phys. Rev. B 52 (1995) 16772.

[3] P.W. Brouwer, C.W.J. Beenakker, Phys. Rev. B 54 (1996) R12705.
[4] S.G. den Hartog et al., Phys. Rev. Lett. 76 (1996) 4592.
[5] S.G. den Hartog et al., Phys. Rev. Lett. 77 (1996) 4954.
[6] S.N. Artemenko, A.F. Volkov, A.V. Zaitsev, Solid State Commun. 30 (1979) 771; S. Yip, Phys. Rev. B 52 (1995) 15504; Y.V. Nazarov, T.H. Stoof, Phys. Rev. Lett. 76 (1996) 823; A.F. Volkov, N. Allsopp, C.J. Lambert, J. Phys.: Condens. Matter. 8 (1996) 45; A.A. Golubov, F.K. Wilhelm, A.D. Zaikin, Phys. Rev. B. 55 (1997) 1123; N. Argaman, Europhys. Lett. 38 (1997) 231.
[7] C.J. Lambert, V.C. Hui, S.J. Robinson, J. Phys. Condens. Matter. 5 (1993) 4187; B.J. van Wees, K.M.H. Lensen, C.J.P.M. Harmans, Phys. Rev. B 44 (1991) 470; M.P. Anantram, S. Datta, Phys. Rev. B 53 (1996) 16390.
[8] N.K. Allsopp et al., J. Phys. Condens. Matter. 6 (1994) 10475.
[9] Here we use that $\langle T^{ee}_{BA}\rangle + \langle T^{he}_{BA}\rangle \simeq 0.5(N - \langle R_{AA}\rangle)$.